

# Phase diagrams and dielectric response of epitaxial barium strontium titanate films: A theoretical analysis

Z.-G. Ban and S. P. Alpay<sup>a)</sup>

*Department of Metallurgy and Materials Engineering and Institute of Materials Science, University of Connecticut, Storrs, Connecticut 06269*

(Received 2 January 2002; accepted for publication 7 March 2002)

We develop phase diagrams for single-domain epitaxial barium strontium titanate films on cubic substrates as a function of the misfit strain based on a Landau–Devonshire phenomenological model similar to the one developed by Pertsev *et al.* [Phys. Rev. Lett. **80**, 1988 (1998)]. The biaxial epitaxy-induced internal stresses enable phase transformations to unusual ferroelectric phases that are not possible in single crystals and bulk ceramics. The dielectric response of the films is calculated as a function of the misfit strain by taking into account the formation of misfit dislocations that relieve epitaxial stresses during deposition. It is shown that by adjusting the misfit strain via substrate selection and film thickness, a high dielectric response can be obtained, especially in the vicinity of structural instabilities. Theoretical estimation of the dielectric constant of (001)  $\text{Ba}_{0.7}\text{Sr}_{0.3}\text{TiO}_3$  and  $\text{Ba}_{0.6}\text{Sr}_{0.4}\text{TiO}_3$  films on (001) Si, MgO,  $\text{LaAlO}_3$ , and  $\text{SrTiO}_3$  substrates as a function of misfit strain and film thickness is provided. An order-of-magnitude increase in the dielectric constant with increasing film thickness is expected for films on  $\text{LaAlO}_3$  and  $\text{SrTiO}_3$  substrates. A structural instability around 40 nm is predicted in films on MgO substrates accompanied by a substantial increase in the dielectric constant. For films on MgO substrates thicker than 40 nm, the analysis shows that the dielectric constant decreases significantly. We show that the theoretical approach not only predicts general trends but is also in good quantitative agreement with the experimental data reported in literature. © 2002 American Institute of Physics. [DOI: 10.1063/1.1473675]

## I. INTRODUCTION

Thin films of barium strontium titanate [ $\text{Ba}_x\text{Sr}_{1-x}\text{TiO}_3$ , (BST)] are of great technological interest due to their desirable ferroelectric and dielectric properties. The high dielectric permittivity offers them the potential of replacing the current silicon oxide and nitride dielectrics in the next generation dynamic random access memories which require higher integration densities.<sup>1,2</sup> In addition, the strong dependence of permittivity on an electric field makes them attractive for application in tunable microwave devices.<sup>3–5</sup> The primary objective of research in ferroelectric thin films has been to reliably reproduce the properties of bulk ceramics or single crystals in thin-film form for device applications. The fundamental problem that limits their use is that ferroelectric films have inferior dielectric, piezoelectric, and pyroelectric properties compared to their bulk counterparts. In some cases, there may be an order of magnitude difference in the electrical and electromechanical properties of the bulk ferroelectric and its thin-film form.<sup>6</sup> This reduction is usually attributed to compositional and microstructural inhomogeneities, defects, and internal stresses.

Internal stresses in thin films arise due to a variety of reasons including the lattice mismatch between film and the substrate in the case of epitaxial films, differences between thermal expansion coefficients (TECs) of film and substrate, and phase transformations. Epitaxy-induced stresses were

shown to have a profound effect on the physical properties of ferroelectric films especially in the vicinity of a phase transformation. For epitaxial single-domain ferroelectric,<sup>7</sup> relaxor ferroelectric,<sup>8,9</sup> and dielectric BST films,<sup>10,11</sup> the role of internal stresses on electrical and electromechanical properties was determined experimentally. It was shown that the choice of substrate and also the film thickness can be used to adjust the internal stress level and thus to tune physical properties. The latter is due to the thickness dependence of stress relaxation by misfit dislocation formation at the deposition temperature.<sup>12,13</sup> For example, for epitaxial films of relaxor ferroelectric  $0.9\text{Pb}(\text{Mg}_{1/3}\text{Nb}_{2/3})\text{O}_3-0.1\text{PbTiO}_3$ , a change of the film thickness from 100 to 400 nm results in almost an order-of-magnitude increase in the dielectric constant and the piezoresponse of the film.<sup>8</sup> Similar results of the effect of internal stresses on physical properties of ferroelectric films were obtained by Chang *et al.*<sup>3,14</sup> and Knauss *et al.*<sup>15</sup> for BST films of various compositions. Furthermore, it was shown that annealing treatments to reduce residual stresses would result in improved dielectric properties and tunability on “compressive” substrates (i.e., substrates with lattice parameters smaller than the film such that compressive stresses are induced in the plane of the film–substrate interface in pseudomorphic films) but not on “tensile” substrates. Shaw *et al.*<sup>16</sup> reported a reduction in dielectric properties in BST films due to tensile residual stresses and investigated the effect of external stress fields as well. Park *et al.*<sup>17</sup> have shown that the stress state and thus the dielectric properties of BST

<sup>a)</sup>Electronic mail: p.alpay@ims.uconn.edu

films can be controlled by depositing very thin, well-matched buffer layers.

Theoretical modeling of the observed dependence of physical properties on misfit strain was carried out using Landau–Devonshire (LD) phenomenology.<sup>3,10,18,19</sup> These models, however, do not take into account the possibility of the formation of different and unusual phases that can not form in bulk ceramics and single crystals due to the internal stresses. This aspect was addressed recently by Pertsev *et al.*,<sup>20</sup> who used a LD thermodynamic model for epitaxial ferroelectric films and predicted the appearance of unusual phases and phase transformations as a result of the epitaxy-induced internal stresses. Misfit strain–temperature phase diagrams were developed for epitaxial BaTiO<sub>3</sub> (BT) and PbTiO<sub>3</sub> (PT) films and the effect of internal stresses on the phase transformation characteristics and the dielectric response was discussed.<sup>20,21</sup>

In this article, we develop similar phase diagrams for single-domain epitaxial (001) Ba<sub>0.6</sub>Sr<sub>0.4</sub>TiO<sub>3</sub> (BST 60/40) and (001) Ba<sub>0.7</sub>Sr<sub>0.3</sub>TiO<sub>3</sub> (BST 70/30) films on (001) cubic substrates as a function of the misfit strain based on the LD phenomenological model in accordance with the one developed by Pertsev *et al.*<sup>20</sup> Our aim is to provide a *quantitative* estimation of the dielectric response as a function of the *misfit strain* as well as the *film thickness* for these two popular BST compositions to serve as a framework for future experimental studies. The article is arranged as follows. Section II provides a very brief summary of the thermodynamic model upon which the misfit strain–temperature phase diagrams of BST 70/30 and BST 60/40 are constructed. In Sec. III, we calculate the theoretical misfit strain of BST 70/30 and BST 60/40 films on popular substrates such as SrTiO<sub>3</sub>, LaAlO<sub>3</sub>, MgO, and Si. Taking into account the relaxation of epitaxial stresses by the formation of misfit dislocations during film growth, we provide a quantitative analysis for the misfit strain as a function of film thickness and subsequently calculate the dielectric response of BST 70/30 and BST 60/40 films on these substrates as a function of film thickness in Sec. IV. A comparison of the theoretical calculations of the dielectric response with experimental results from literature is also presented. Finally, we discuss the limitations and the approximations used in the theoretical calculations as well as the behavior of the spontaneous polarization of BST films on tensile substrates as a function of film thickness, which resembles the size effect in ferroelectric particles as a function of particle size.

## II. THE MISFIT STRAIN–TEMPERATURE PHASE DIAGRAM FOR BST FILMS

To construct the misfit–temperature phase diagram for BST films, we consider the case of a single-domain (001) BST film epitaxially grown in the cubic paraelectric phase on a thick (001) cubic substrate under short-circuit electrical boundary conditions. In this case, the thermodynamic potential  $\tilde{G}$  of the pseudocubic BST film as a function of polarization  $P_i$ , misfit strain  $u_m = (a_S - a_0)/a_S$ , where  $a_S$  is the

TABLE I. The parameters for the calculation of the renormalized coefficients for BST films. Data compiled from Refs. 20, 22–25;  $T_C$ : Curie temperature,  $C$ : Curie constant,  $A_{ij}$ : stiffness coefficients,  $S_{ij}$ : elastic compliances, and  $Q_{ij}$ : electrostrictive coefficients.

Parameter	BST 70/30	BST 60/40
$T_C$ (°C)	34	5
$C$ (10 <sup>5</sup> °C)	1.29	1.22
$a_{11}$ (10 <sup>6</sup> m <sup>5</sup> /C <sup>2</sup> F)	2.52 $T$ + 189 ( $T$ in °C)	2.16 $T$ + 462 ( $T$ in °C)
$a_{12}$ (10 <sup>8</sup> m <sup>5</sup> /C <sup>2</sup> F)	7.21	7.98
$S_{11}$ (10 <sup>-12</sup> m <sup>2</sup> /N)	5.92	5.12
$S_{12}$ (10 <sup>-12</sup> m <sup>2</sup> /N)	-1.92	-1.65
$S_{44}$ (10 <sup>-12</sup> m <sup>2</sup> /N)	6.7	5.86
$Q_{11}$ (m <sup>4</sup> /C <sup>2</sup> )	0.1	0.1
$Q_{12}$ (m <sup>4</sup> /C <sup>2</sup> )	-0.034	-0.034
$Q_{44}$ (m <sup>4</sup> /C <sup>2</sup> )	0.029	0.029

substrate lattice parameter and  $a_0$  is the equivalent cubic cell constant of the free standing film, and the temperature  $T$ , can be written in a renormalized form as<sup>20</sup>

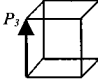
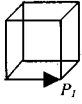
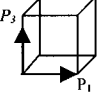
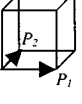
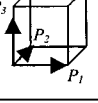
$$\begin{aligned} \tilde{G} = & a_1^* (P_1^2 + P_2^2) + a_3^* P_3^2 + a_{11}^* (P_1^4 + P_2^4) + a_{33}^* P_3^4 \\ & + a_{13}^* (P_1^2 P_3^2 + P_2^2 P_3^2) + a_{12}^* P_1^2 P_2^2 + a_{111} (P_1^6 + P_2^6 \\ & + P_3^6) + a_{112} [P_1^4 (P_2^2 + P_3^2) + P_3^4 (P_1^2 + P_2^2) + P_2^4 (P_1^2 \\ & + P_3^2)] + a_{123} P_1^2 P_2^2 P_3^2 + \frac{u_m^2}{S_{11} + S_{12}}. \end{aligned} \quad (1)$$

The renormalized coefficients of the free energy expansion are given by

$$\begin{aligned} a_1^* &= a_1 - u_m \frac{Q_{11} + Q_{12}}{S_{11} + S_{12}}, \quad a_3^* = a_1 - u_m \frac{2Q_{12}}{S_{11} + S_{12}}, \\ a_{11}^* &= a_{11} + \frac{1}{2} \frac{1}{S_{11}^2 - S_{12}^2} [(Q_{11}^2 + Q_{12}^2)S_{11} - 2Q_{11}Q_{12}S_{12}], \\ a_{33}^* &= a_{11} + \frac{Q_{12}^2}{S_{11} + S_{12}}, \\ a_{12}^* &= a_{12} - \frac{1}{S_{11}^2 - S_{12}^2} [(Q_{11}^2 + Q_{12}^2)S_{12} - 2Q_{11}Q_{12}S_{11}] \\ & \quad + \frac{Q_{44}^2}{2S_{44}}, \\ a_{13}^* &= a_{12} + \frac{Q_{12}(Q_{11} + Q_{12})}{S_{11} + S_{12}}, \end{aligned} \quad (2)$$

where  $a_1$  is the dielectric stiffness,  $a_{ij}$  and  $a_{ijk}$  are higher order stiffness coefficients at constant stress,  $Q_{ij}$  are the electrostrictive coefficients, and  $S_{ij}$  are the elastic compliances of the film. The temperature dependence of the dielectric stiffness  $a_1$  is given by the Curie–Weiss law,  $a_1 = (T - T_0)/2\epsilon_0 C$  where  $T_0$  and  $C$  are the Curie–Weiss temperature and constant of a bulk ferroelectric, respectively, and  $\epsilon_0$  is the permittivity of free space. The parameters used for the calculation of the renormalized coefficients for BST films are obtained by averaging the corresponding parameters of BaTiO<sub>3</sub> and SrTiO<sub>3</sub> as given in Table I.<sup>20,22–25</sup> Both  $a_1$  and  $a_{11}$  are temperature dependent in BST since both scale with

TABLE II. The polarization components of the theoretically predicted phases in epitaxial ferroelectric thin films (after Ref. 20).

Phase	Polarization components	
Paraelectric	$P_1 = P_2 = P_3 = 0$	
<i>c</i> phase	$P_1 = P_2 = 0, P_3 \neq 0$	
<i>a</i> phase	$P_1 \neq 0, P_2 = P_3 = 0$	
<i>ac</i> phase	$P_1 \neq 0, P_2 = 0, P_3 \neq 0$	
<i>aa</i> phase	$P_1 = P_2 \neq 0, P_3 = 0$	
<i>r</i> phase	$P_1 = P_2 \neq 0, P_3 \neq 0$	

temperature in BaTiO<sub>3</sub>. All other parameters in Table I are assumed to be temperature independent in the range investigated. In our calculations, the contribution of six-order polarization terms to the free energy is neglected.<sup>26</sup> To determine equilibrium thermodynamic states of the BST film, we calculate the minima of  $\tilde{G}(P_i, u_m, T)$  with respect to the components of the polarization for all possible six phases in epitaxial films as identified by Pertsev *et al.*<sup>20</sup> at a given temperature and misfit strain. The polarization components of the six phases are listed in Table II.<sup>20</sup> The phase that has the minimum free energy was selected as the stable phase.

We have performed the analysis for BST 70/30 and BST 60/40 films and the resulting misfit–temperature phase diagrams are shown in Fig. 1. These compositions are the most

widely investigated compositions because their Curie temperature is very close to room temperature ( $T_C = 34^\circ\text{C}$  and  $5^\circ\text{C}$  for BST 70/30 and BST 60/40, respectively) and due to the proximity to the ferroelectric–paraelectric phase transformation, a large dielectric constant is expected. Some distinct features of the phase diagrams can be summarized as follows:

- (1) The phases occurring for both films in the examined temperature and misfit strain range are the paraelectric phase, the *c* phase, the *r* phase and the *aa* phase. The unusual *r* phase that is forbidden in single crystals and bulk ceramics appears in epitaxial thin films at a particular misfit-strain range, indicating that the misfit strain in thin films may alter the type of the stable ferroelectric phase with respect to that in unconstrained ceramics and single crystals of the same composition. Positive misfit strain (i.e., tensile stress) favors the appearance of the *aa* phase which has in-plane polarizations, while the negative misfit strain (i.e., compressive stress) induces the *c* phase which has the polarization vector perpendicular to the film/substrate interface.
- (2) Our calculation indicates that all the phase transformations in constrained BST films are of the second order due to the positive sign of the coefficients  $a_{11}^*$ ,  $a_{12}^*$ ,  $a_{13}^*$ , and  $a_{33}^*$ . This agrees with the examination of the polarization components of the ferroelectric phases as a function of misfit strain for BST 70/30 film at room temperature, as shown in Fig. 2. The polarization components of the various phases are given by

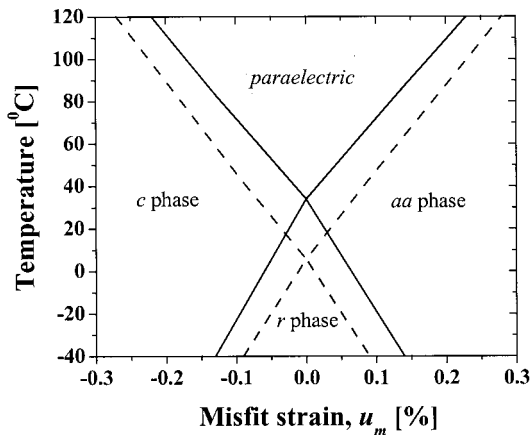


FIG. 1. Phase diagrams of (001) single-domain BST 70/30 (solid line) and BST 60/40 (dashed line) thin films epitaxially grown on the cubic substrate.

$$c \text{ phase: } P_3^2 = P_c^2 = -\frac{a_3^*}{2a_{33}^*},$$

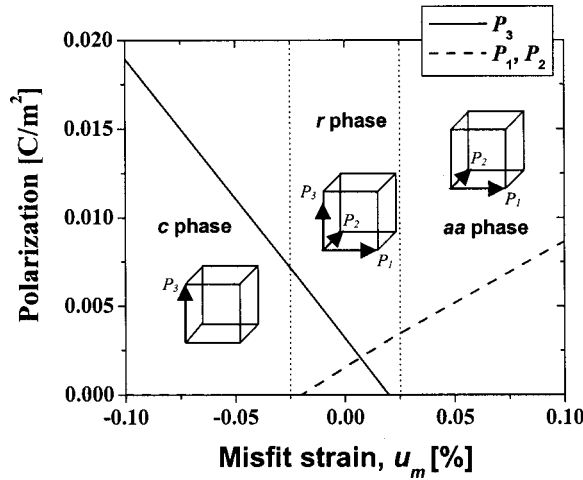


FIG. 2. Polarization components of the ferroelectric phases as a function of misfit strain for BST 70/30 at room temperature.

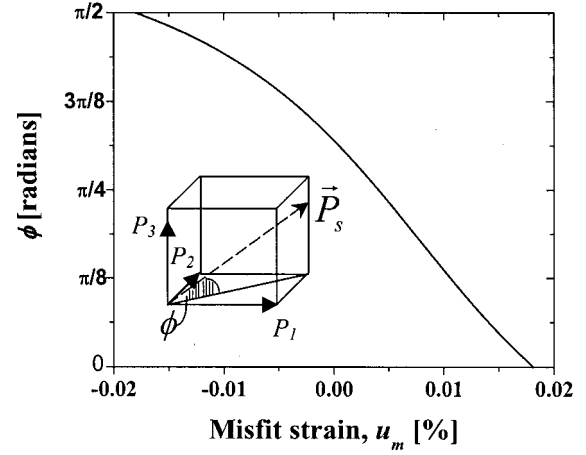


FIG. 3. Angle  $\phi$  between the spontaneous polarization  $P_s$  ( $P_s = \sqrt{2P_1^2 + P_3^2}$ ) of  $r$  phase and the film/substrate normal [001] direction as a function of misfit strain for BST 70/30 film at RT ( $T=25^\circ\text{C}$ ).

$$\begin{aligned}
 \text{aa phase: } P_1^2 = P_2^2 = P_{aa}^2 &= -\frac{a_1^*}{2a_{11}^* + a_{12}^*} \\
 r \text{ phase: } P_1^2 = P_2^2 = P_{r1}^2 &= \frac{a_{13}^* a_3^* - 2a_{11}^* a_{33}^*}{4a_{11}^* a_{33}^* + 2a_{12}^* a_{33}^* - 2a_{13}^{*2}}, \\
 P_3^2 = P_{r3}^2 &= \frac{2a_{13}^* a_1^* - 2a_{11}^* a_3^* - a_{12}^* a_3^*}{4a_{11}^* a_{33}^* + 2a_{12}^* a_{33}^* - 2a_{13}^{*2}}. \quad (3)
 \end{aligned}$$

It can be seen from Fig. 2 that with the increase of the misfit strain from negative to positive values, the  $P_3$  component decreases to zero and  $P_1(=P_2)$  increases from zero to nonzero values in a continuous fashion. There is no jump for the polarization components at the phase boundaries.

- (3) The Curie temperature, where the transition from paraelectric state to a ferroelectric state occurs, is shifted as a result of the misfit strain. Both positive and negative misfit strains lead to an increase in the Curie temperature. The same trend was also observed in the misfit-temperature diagrams of BT and PT.<sup>20</sup>
- (4) The  $r$  phase is monoclinic which has polarization components along all the three crystal axes ( $P_1 = P_2 \neq 0, P_3 \neq 0$ ). Therefore, a rotation of the polarization vector from the [001] direction of the film is expected with increasing tensile misfit strain. Figure 3 shows the angle  $\phi$  between the spontaneous polarization  $P_s$  ( $P_s = \sqrt{2P_1^2 + P_3^2}$ ) of the  $r$  phase and the film/substrate normal [001] direction as a function of misfit strain for BST 70/30 film at room temperature (RT=25 °C). It can be seen from Fig. 3 that the spontaneous polarization of the  $r$  phase rotates 90° from the [001] direction into the [110] direction at the misfit range in which the  $r$  phase is stable. Since the spontaneous polarization of the  $c$  phase and the  $aa$  phase are along [001] and [110] directions, respectively, both of the transformations from the  $c$  phase to the  $r$  phase and from the  $r$  phase to the  $aa$  phase are of second order, which is consistent with the prediction from the phase diagram.

### III. EFFECT OF SUBSTRATE SELECTION AND FILM THICKNESS ON THE PHASE TRANSFORMATION

The obvious way to adjust the misfit strain in the heteroepitaxial films is by the selection of a substrate material. BST films are usually deposited at temperatures exceeding 600 °C and thus, it is important to take into account the thermal stresses that may develop upon cooling down from the growth temperature  $T_G$  due to the difference between the TECs of the film and the substrate. However, suitable substrate materials are limited in that they have to match reasonably well in terms of their lattice constants and TECs with the film to ensure epitaxial growth.

Systematic variations in the internal stress level of heteroepitaxial films can be achieved by altering the film thickness. The epitaxial stresses are relaxed to a certain extent by the formation of misfit dislocations at  $T_G$ . The equilibrium thermodynamic theory of misfit dislocations was developed by van der Merwe<sup>12</sup> and Matthews and Blakeslee<sup>13</sup> and is now well established.<sup>27,28</sup> The theory predicts a critical thickness  $h_\rho$  below which the formation of misfit dislocations is not feasible. The effective misfit strain at the deposition temperature,  $u_m(T_G) = u_m^0$ , scales with the film thickness  $h$  as<sup>28,29</sup>

$$u_m^0 = \rho a_0(T_G) \left(1 - \frac{h_\rho}{h}\right)^{-1}, \quad (4)$$

where  $\rho$  is the equilibrium linear misfit dislocation density at  $T_G$ . Therefore, another way to control the misfit strain in heteroepitaxial films is via varying the thickness of the deposit. Assuming no additional dislocations form during cooling down [i.e.,  $\rho(T_G) = \rho(T)$  for  $T < T_G$ ], an “effective” substrate lattice parameter,  $\bar{a}_s$ , can be defined and used for the calculation of the misfit strain of the films with a different thickness grown on a selected substrate.<sup>29,30</sup>

$$\bar{a}_s(T) = \frac{a_s(T)}{\rho a_s(T) + 1}. \quad (5)$$

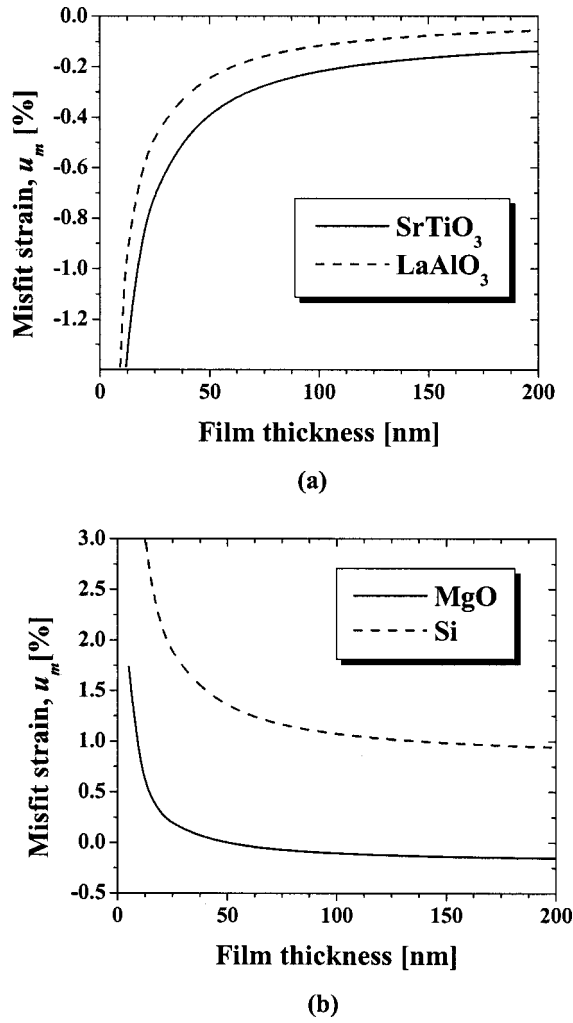


FIG. 4. Misfit strain of BST 60/40 films on various substrates as a function of film thickness at room temperature ( $T = 25^\circ\text{C}$ ). (a) SrTiO<sub>3</sub> and LaAlO<sub>3</sub> (compressive substrates), and (b) MgO and Si (tensile substrates).

To provide a quantitative estimation of the physical properties of BST films, we have chosen four popular substrate materials: SrTiO<sub>3</sub>, LaAlO<sub>3</sub>, MgO, and Si. The lattice parameters of the substrates, BST 70/30, and BST 60/40 and their respective thermal expansion coefficients are given in Table III.<sup>10,14,22,31–33</sup> The substrates investigated can be classified into two categories: compressive substrates and tensile substrates (i.e., substrates with lattice parameters smaller or larger than the film such that in pseudomorphic films compressive or tensile stresses are induced in the plane of the film–substrate interface, respectively). Accordingly, SrTiO<sub>3</sub> and LaAlO<sub>3</sub> are compressive and MgO and Si are tensile substrates for BST 70/30 and BST 60/40. Assuming that  $T_G = 800^\circ\text{C}$ , in Fig. 4, we plot the variation in the theoretical misfit strain at RT of BST 60/40 films on these substrates as a function of film thickness. Since the lattice parameter and TEC of BST 70/30 are very close to the ones of BST 60/40 (see Table III), BST 70/30 films exhibit almost identical behavior with minor variations in the magnitude of the misfit strain and are therefore not included. The critical thicknesses for dislocation formation  $h_p$  are calculated to be 10.7 nm, 2.5 nm, 1.6 nm, and 1 nm for BST 70/30, and 11.8 nm, 2.6 nm,

TABLE III. Lattice parameters of substrates, BST 70/30, and BST 60/40 at RT and their respective TECs. Data compiled from Refs. 10, 14, 22, 31–33.

Substrate	Lattice parameter (nm)	TEC ( $\times 10^{-6}^\circ\text{C}^{-1}$ )
BST 70/30	0.3965	10.5
BST 6040	0.3960	10.5
MgO	0.4211	13.47
LaAlO <sub>3</sub>	0.3787	10.0
SrTiO <sub>3</sub>	0.3904	11.0
Si	0.5431	$3.725 \times \{1 - \exp[-5.88 \times 10^3(T+149)]\}$ $+ 5.548 \times 10^{-4} \times (T+273)$

1.5 nm, and 1 nm for BST 60/40 on SrTiO<sub>3</sub>, LaAlO<sub>3</sub>, MgO, and Si substrates, respectively. It can be seen from Fig. 4 that the magnitude of misfit strains of the films on all the four substrates decreases dramatically with the increase of the film thickness owing to the relaxation by the misfit dislocation formation, regardless whether the substrate is compressive or tensile. The misfit strain may be fully relaxed at a certain film thickness as for MgO substrate. In fact, compressive misfit strains may be expected for MgO substrates for films thicker than  $\sim 52$  nm [see Fig. 4(b)] due to the interplay between the misfit strain relaxation by interfacial dislocations at  $T_G$  and the developing thermal stresses due to the difference in the TECs of the film and the substrate as the film is cooled from  $T_G$  to RT.

The consequence of the strain relaxation by the misfit dislocation formation is that a phase transition may occur as the film thickness increases. For example, as indicated by the BST 60/40 phase diagram (Fig. 1), there is a narrow misfit strain region ( $-0.06\% - 0.06\%$ ) corresponding to the paraelectric phase region at RT. Thus, as the misfit strain goes down with an increase of the film thickness, the film may be in the paraelectric state, rather than  $c$  phase for compressive substrates [Fig. 4(a)] and  $aa$  phase for tensile substrates [Fig. 4(b)]. Therefore, by the selection of the substrate material and film thickness, the level and sign of the misfit strain can be adjusted as to obtain optimum dielectric response which will be discussed in the next section.

#### IV. DIELECTRIC RESPONSE

Figure 5 shows the calculated dependence of the small-signal dielectric constant on the misfit strain at RT. The relative dielectric constants along the normal of the film/substrate interface  $\epsilon_{33}$  and parallel with the film/substrate interface  $\epsilon_{11}$  are chosen for the BST 70/30 film and BST 60/40 film, respectively. The relative dielectric constants are related to the inverse of second derivative of  $\tilde{G}$  [Eq. (1)] with respect to the polarization components  $P_i$  of the phases and are given by

$$c \text{ phase: } \frac{\epsilon_{33}}{\epsilon_0} = -\frac{1}{4\epsilon_0 a_3^*},$$

$$\frac{\epsilon_{11}}{\epsilon_0} = \frac{a_{33}^*}{\epsilon_0(2a_1^* a_{33}^* - a_{13}^* a_3^*)}, \quad (6)$$

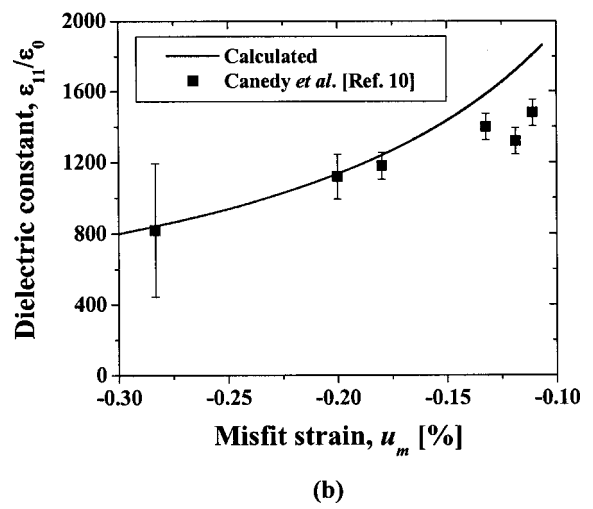
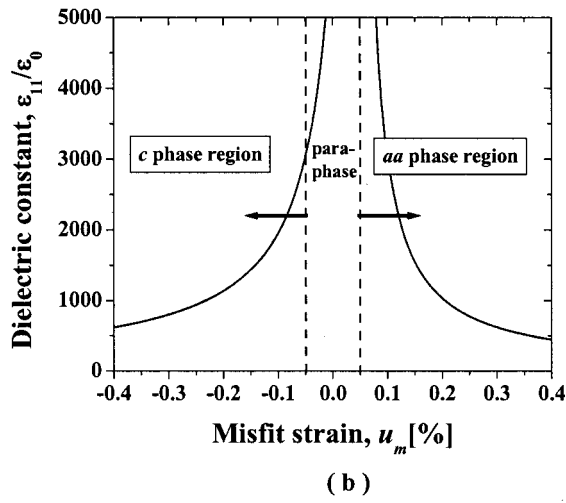
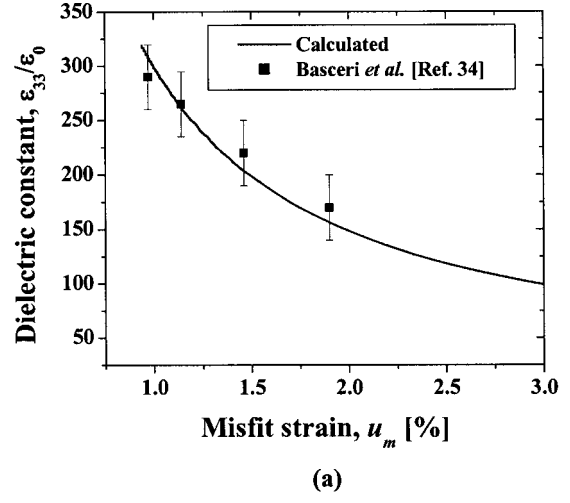
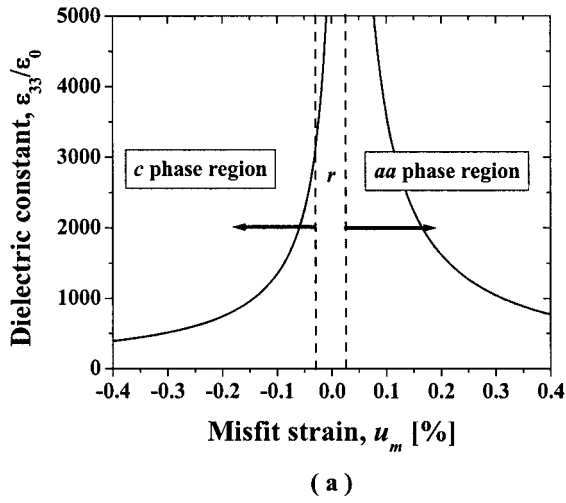


FIG. 5. Calculated dependence of the dielectric constant on the misfit strain at RT. (a)  $\epsilon_{33}/\epsilon_0$  of BST 70/30 film. (b)  $\epsilon_{11}/\epsilon_0$  of BST 60/40 film.

FIG. 6. The comparison between the theoretical calculations of dielectric constant (solid lines) with the reported experimental results (solid squares). (a)  $\epsilon_{33}/\epsilon_0$  of BST 70/30 film. (b)  $\epsilon_{11}/\epsilon_0$  of BST 60/40 film.

$$\text{paraelectric phase: } \frac{\epsilon_{33}}{\epsilon_0} = \frac{1}{2\epsilon_0 a_3^*}, \quad \frac{\epsilon_{11}}{\epsilon_0} = \frac{1}{2\epsilon_0 a_1^*}, \quad (7)$$

$$r \text{ phase: } \frac{\epsilon_{33}}{\epsilon_0} = \frac{1}{2\epsilon_0(a_3^* + 2a_{13}^*P_{r_1}^2 + 6a_{33}^*P_{r_3}^2)},$$

$$\frac{\epsilon_{11}}{\epsilon_0} = \frac{1}{2\epsilon_0[a_1^* + a_{13}^*P_{r_3}^2 + (a_{12}^* + 6a_{11}^*)P_{r_1}^2]}, \quad (8)$$

$$aa \text{ phase: } \frac{\epsilon_{33}}{\epsilon_0} = \frac{1}{2\epsilon_0(a_3^* + 2a_{13}^*P_{aa}^2)},$$

$$\frac{\epsilon_{11}}{\epsilon_0} = \frac{1}{2\epsilon_0[a_1^* + (a_{12}^* + 6a_{11}^*)P_{aa}^2]}, \quad (9)$$

where the spontaneous polarization  $P_{r_1}$ ,  $P_{r_3}$ , and  $P_{aa}$  for  $r$  phase and  $aa$  phase are given in Eq. (3). The stable regions in accordance with the phase diagram are also indicated in Fig. 5. The characteristic feature of Fig. 5 is that the dielectric constant exhibits anomaly in the misfit dependence for both of the films. Such a dielectric anomaly occurs at the phase boundaries, i.e., the  $r$  phase / the  $aa$  phase for BST 70/30 and *paraelectric* /  $aa$  phase for BST 60/40. The behavior of the

dielectric properties of BST films is related to the “structural instabilities,” as demonstrated in BT and PT systems.<sup>20</sup>

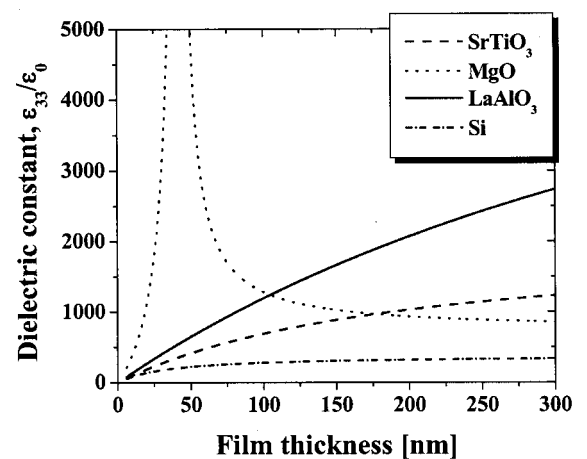
The aforementioned theoretical prediction of the dielectric properties of single-domain BST 70/30 film and BST 60/40 film may be compared with the experimental results published in literature, as illustrated in Fig. 6. The experimental result shown in Fig. 6(a) was obtained for highly textured BST 70/30 films grown on Si substrates reported by Basceri *et al.*<sup>34</sup> BST 70/30 films were deposited at approximately 640 °C on Pt-coated Si wafers by a liquid-delivery-source chemical vapor deposition technique, to thicknesses ranging from 24 to 160 nm. The resulting films had a columnar microstructure and were strongly {100} textured. Basceri *et al.*<sup>34</sup> utilized the interfacial capacitance model to elucidate the observed dielectric permittivity dependence on the film thickness but the observed behavior may be the effect of the dependence of internal stresses on the film thickness due to misfit dislocation formation at  $T_G$ . Assuming that the grain size of the films  $D$  is larger than film thickness  $h$  (i.e.,  $D/h > 1$ ) in the highly textured film, the textured film may be treated as an epitaxial film. This assumption enables us to compare the aforementioned experimental results with our

theoretical calculation. To perform this, the misfit strain data were first retrieved from film thickness data reported in Ref. 34 using the methodology described in Sec. III, then combinations of misfit strain and dielectric constant were established, as represented by the solid squares in Fig. 6(a). Our analysis shows that the BST 70/30 film grown on the Si substrate falls into *aa* phase region which has prevailing in-plane polarization. Taking this point into account, the calculated dielectric constant  $\epsilon_{33}$  fits the experimental data reasonably well.

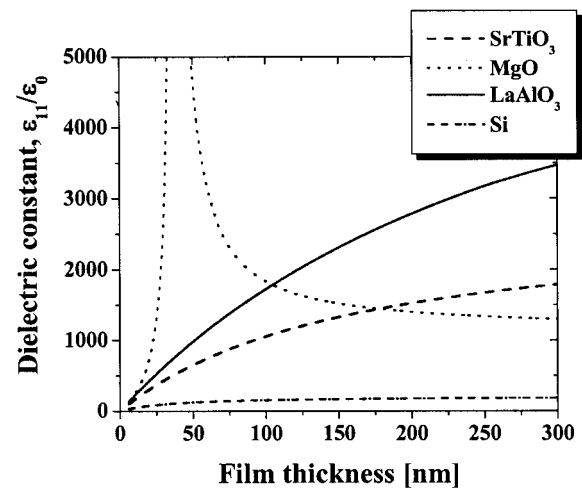
Experimental data shown in Fig. 6(b) were obtained by Canedy *et al.*<sup>10</sup> who investigated the effect of misfit strain on the dielectric properties of (001) BST 60/40 films grown on (001) 0.29(LaAlO<sub>3</sub>):0.35(Sr<sub>2</sub>TaAlO<sub>6</sub>) substrates. The BST 60/40 films were fabricated using pulsed-laser deposition (PLD) with the substrate temperature held at 800 °C during deposition and a dynamic pressure of 120 mTorr O<sub>2</sub> established in the chamber. The in-plane dielectric constants  $\epsilon_{11}$  of the resulting films were mapped as a function of film thickness. On the basis of the discussion in Sec. III, a compressive misfit strain develops in this case and the film virtually falls into the *c* phase region in which the spontaneous polarization is lined up perpendicular to the film/substrate interface. It can be seen from Fig. 6(b) that our theoretical calculations of the dielectric constant dependence on the misfit strain are in excellent agreement with the experimental results.

As discussed herein, the phase transformation induced by the misfit strain greatly influences the dielectric response of BST films. Taking into account the strain relaxation by misfit dislocation formation, the misfit strain could be correlated with the film thickness for different substrates, as presented in Sec. III. As such, the substrate materials and film thickness may be chosen as the design parameters to adjust the misfit strain state in the film and to manipulate the dielectric response. Figures 7(a) and 7(b) show the dependence of calculated dielectric constant  $\epsilon_{33}/\epsilon_0$  and  $\epsilon_{11}/\epsilon_0$  on the film thickness for BST 70/30 films and for BST 60/40 films on various substrates at RT, respectively. Close examination of Fig. 7 reveals that except for MgO substrates, the films on SrTiO<sub>3</sub>, LaAlO<sub>3</sub>, and Si substrates display the same trend, i.e., an increase in the dielectric constant with an increase of the film thickness. This is attributed to the fact that the films on these substrates are in the single-phase region in the thickness range evaluated. For example, films on SrTiO<sub>3</sub> stay in the *c* phase region due to the compressive strain regardless of the film thickness. Interestingly, the dielectric response of the films on Si substrates is remarkably small compared with those of the films on the SrTiO<sub>3</sub> and LaAlO<sub>3</sub> substrates, due to the large tensile misfit strain ( $\sim 1\%$ ) even with strain relaxation by misfit dislocation formation. Since dielectric constants increase steadily as film thickness increases for films on SrTiO<sub>3</sub> and LaAlO<sub>3</sub> substrates, films should be as thick as possible in order to achieve optimum dielectric response.

For films on the MgO substrates, however, the dielectric response behaves significantly differently in comparison with the other three substrates. A dielectric constant anomaly is observed at a critical thickness of  $\sim 40$  nm, which is associated with the transformation from *aa* phase to *r* phase for BST 70/30 film. The theoretical analysis shows that the di-



(a)



(b)

FIG. 7. Dependence of calculated dielectric constant on the film thickness for films on various substrates at RT. (a)  $\epsilon_{33}/\epsilon_0$  for BST 70/30 films and (b)  $\epsilon_{11}/\epsilon_0$  for BST 60/40.

electric constant decreases substantially with increasing film thickness. The exact same trend was observed experimentally in (001) BST 50/50 film grown on (001) MgO substrate by PLD at 800 °C where a drop in  $\epsilon_{11}/\epsilon_0$  from 2350 to 1700 was reported as the film thickness was increased from 14 to 500 nm.<sup>11</sup> This result suggests that a large dielectric constant in BST 70/30 on MgO substrates may be achieved by decreasing the film thickness to the vicinity of the critical film thickness at which a structural instability related to the *aa-r* phase transformation is expected.

## V. DISCUSSION OF RESULTS

As pointed out in previous sections, the misfit-temperature phase diagram for BST films developed can be utilized to predict the strain induced phase transformations that may affect the dielectric properties of the films profoundly. However, there are some limitations for the developed phase diagrams as discussed next.

First of all, the coefficients in the free energy expansion for BST film are obtained by simply averaging the corresponding free energy expansion coefficients and the elastic

moduli of  $\text{BaTiO}_3$  and  $\text{SrTiO}_3$  due to the lack of data on single crystals of the same composition. This approximation may introduce some errors since the coefficients may not be the linear function of the Ba/Sr ratio. The good correlation between the theoretical results and experimental results leads us to believe that this approach may be a reasonable approximation for the physical properties of BST films. Secondly, the  $P^4$  approximation is used in the free energy expansion and the six-order polarization terms are neglected. This approximation remains valid as long as the temperature is not far below the Curie temperature. The six-order terms can become important when the temperature is well below the Curie temperature.<sup>35</sup> Furthermore, in our analysis, we have limited ourselves to a temperature range from  $-40^\circ\text{C}$  to  $120^\circ\text{C}$ . We have not taken into account the possibility of the formation of structural domains, or twins, due to the extremely small self-strain of the paraelectric–ferroelectric phase transformation in BST 60/40 and BST 70/30 films in the investigated temperature interval. The formation of certain polydomain structures such as the  $a_1/a_2/a_1/a_2$  pattern which consists of transversely modulated thin platelets of  $a_1$  domains and  $a_2$  domains with the  $c$  axis of the tetragonal film along the  $[100]$  or  $[010]$  directions of the substrate, respectively, is thermodynamically possible for relatively large tensile misfit strains.<sup>28,29,36–42</sup> However, there is no experimental observation of any kind of polydomain structure in epitaxial BST 70/30 and BST 60/40 films. And finally, there are also limitations to the thermodynamic modeling of the effect of misfit dislocations. The theoretical approach of Matthews and Blakeslee<sup>13</sup> is based on the elastic continuum concept only and neglects the interaction of misfit dislocation with the dislocations present in the film. Additionally, the real critical thickness for dislocation formation and the linear equilibrium dislocation density may differ significantly from the actual observed values because of kinetic factors.<sup>27,43,44</sup> Therefore, it is necessary to measure the actual misfit strain which can be done via x-ray diffraction by comparing the peak position of the diffraction from the film to its unconstrained position.

One interesting aspect of the theoretical analysis is presented in Fig. 8, where we plot the  $[001]$  component of the polarization ( $P_3$ ) as a function of film thickness for (001) BST 70/30 films on (001)  $\text{SrTiO}_3$ ,  $\text{LaAlO}_3$ , and  $\text{MgO}$  at RT. For films on Si, the  $aa$  phase is stable throughout the investigated film thickness range and thus there is no  $P_3$  component of the polarization.  $P_3$  decreases with film thickness for films on compressive substrates ( $\text{SrTiO}_3$  and  $\text{LaAlO}_3$ ) due to relaxation of compressive stresses by misfit dislocations with increasing film thickness [see Fig. 4(a)]. On the other hand, for films on  $\text{MgO}$  substrates, a decline in  $P_3$  is expected with decreasing film thickness due to increasing tensile misfit strain as a function of the film thickness [see Fig. 4(b)]. This results in the gradual rotation of the polarization vector from the  $[001]$  direction towards the (001) plane ( $r$  phase). Below a critical thickness of  $\sim 40$  nm, the film is in the  $aa$  phase region with no  $P_3$  component as a result of tensile misfit strain.

The behavior resembles the so-called size effect in ferroelectric particles which refers to the suppression of ferroelec-

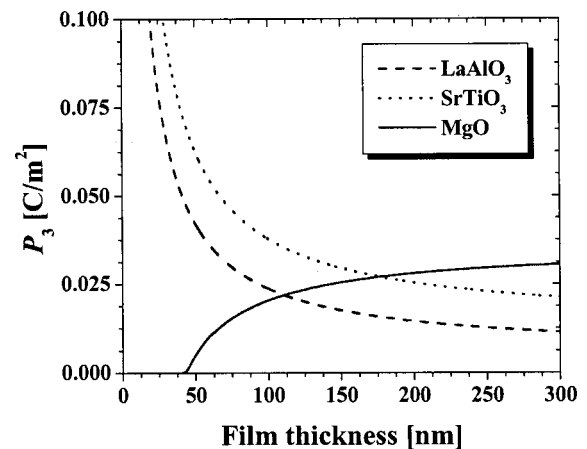


FIG. 8. Polarization component normal to the film/substrate interface ( $P_3$ ) as a function of film thickness for BST 70/30 films on various substrates at room temperature.

tricity below a critical particle size due to surface effects or depolarization fields.<sup>6,45–47</sup> For ferroelectric thin films, phenomenological models were developed which indicate a critical thickness below which the ferroelectricity is suppressed.<sup>48–50</sup> However, first-principles calculations of ferroelectricity in PT films under stress-free and short-circuit conditions show that films with thickness as low as a couple of unit cell dimensions exhibit ferroelectricity with significant enhancement of the polarization at the surface.<sup>51</sup> Experimentally, lead zirconate titanate films were observed to exhibit ferroelectricity down to 4 nm film thickness.<sup>52</sup> Very recently, size driven phase transformations in ferroelectric thin films under biaxial stresses have been analyzed using a phenomenological approach.<sup>50</sup> However, this model has not considered that the internal stress is also a function of film thickness due to relaxation by misfit dislocations. Obviously, the theoretical polarization response illustrated in Fig. 8 is obtained without considering the surface effects or depolarization fields. However, it suggests that epitaxy-induced internal stresses that are a function of the film thickness may yield, in certain cases, results that are very similar to the size effect. Therefore, epitaxial stresses should be taken into account in the analysis of the size effect especially for “soft” ferroelectric thin films with a small self-strain of the paraelectric–ferroelectric transformation and/or close to the transformation temperature.

## VI. CONCLUSION

We have examined the effect of misfit strain on phase transformations of the single-domain epitaxial barium strontium titanate films on cubic substrates. The misfit strain–temperature phase diagrams for BST 70/30 and BST 60/40 have been established on the basis of a LD phenomenological theory developed by Pertsev *et al.*<sup>20</sup> We have quantitatively analyzed the dielectric response of the BST 70/30 and BST 60/40 films as a function of the misfit strain and film thickness. The dielectric constants of both films exhibit an anomaly in the misfit strain dependence due to phase transformations. The calculated dielectric properties are in good agreement with the experimental data reported in literature.

The selection of the substrate and/or the film thickness can be chosen as design parameters to manipulate the strain state in the film to achieve optimum dielectric response.

## ACKNOWLEDGMENTS

The authors gratefully acknowledge support from the National Science Foundation (NSF) under Grant No. DMR-0132918 and the University of Connecticut Research Foundation.

- <sup>1</sup>S. Summerfelt, in *Thin Film Ferroelectric Materials and Devices*, edited by R. Ramesh (Kluwer, Boston, 1997), p. 1.
- <sup>2</sup>A. I. Kingon, S. K. Streiffer, C. Basceri, and S. R. Summerfelt, *Mater. Res. Bull.* **46**, (1996).
- <sup>3</sup>W. Chang, C. M. Gilmore, W.-J. Kim, J. M. Pond, S. W. Kirchoefer, S. B. Qadri, D. B. Chrisey, and J. S. Horwitz, *J. Appl. Phys.* **87**, 3044 (2000).
- <sup>4</sup>J. Im, O. Auciello, P. K. Baumann, S. K. Streiffer, D. Y. Kaufman, and A. R. Krauss, *Appl. Phys. Lett.* **76**, 625 (2000).
- <sup>5</sup>C. L. Chen, J. Shen, S. Y. Chen, G. P. Luo, C. W. Chu, F. A. Miranda, F. W. Van Keuls, J. C. Jiang, E. I. Meletis, and H. Y. Chang, *Appl. Phys. Lett.* **78**, 652 (2001).
- <sup>6</sup>T. M. Shaw, S. Trolrier-McKinstry, and P. C. McIntyre, *Annu. Rev. Mater. Sci.* **30**, 263 (2000).
- <sup>7</sup>A. L. Roytburd, S. P. Alpay, V. Nagarajan, C. S. Ganpule, S. Aggarwal, E. D. Williams, and R. Ramesh, *Phys. Rev. Lett.* **85**, 190 (2000).
- <sup>8</sup>V. Nagarajan, C. S. Ganpule, B. Nagaraj, S. Aggarwal, S. P. Alpay, A. L. Roytburd, E. D. Williams, and R. Ramesh, *Appl. Phys. Lett.* **75**, 4183 (1999).
- <sup>9</sup>V. Nagarajan, S. P. Alpay, C. S. Ganpule, B. Nagaraj, S. Aggarwal, E. D. Williams, A. L. Roytburd, and R. Ramesh, *Appl. Phys. Lett.* **77**, 438 (2000).
- <sup>10</sup>C. L. Canedy, H. Li, S. P. Alpay, L. Salamanca-Riba, A. L. Roytburd, and R. Ramesh, *Appl. Phys. Lett.* **77**, 1695 (2000).
- <sup>11</sup>H. Li, A. L. Roytburd, S. P. Alpay, T. D. Tran, L. Salamanca-Riba, and R. Ramesh, *Appl. Phys. Lett.* **78**, 2354 (2001).
- <sup>12</sup>J. H. van der Merve, *J. Appl. Phys.* **34**, 123 (1963).
- <sup>13</sup>J. W. Matthews and A. E. Blakeslee, *J. Cryst. Growth* **27**, 118 (1974).
- <sup>14</sup>W. Chang, J. S. Horwitz, A. C. Carter, J. M. Pond, S. W. Kirchoefer, C. M. Gilmore, and D. B. Chrisey, *Appl. Phys. Lett.* **74**, 1033 (2000).
- <sup>15</sup>L. A. Knauss, J. M. Pond, J. S. Horwitz, D. B. Chrisey, C. H. Mueller, and R. Treece, *Appl. Phys. Lett.* **69**, 25 (1996).
- <sup>16</sup>T. M. Shaw, Z. Suo, M. Huang, E. Liniger, R. B. Laibowitz, and J. D. Baniecki, *Appl. Phys. Lett.* **75**, 2129 (1999).
- <sup>17</sup>B. H. Park, E. J. Peterson, Q. X. Jia, J. Lee, W. Si, and X. X. Xi, *Appl. Phys. Lett.* **78**, 533 (2001).
- <sup>18</sup>G. A. Rossetti Jr., L. E. Cross, and K. Kushida, *Appl. Phys. Lett.* **59**, 2524 (1991).
- <sup>19</sup>S. H. Oh and H. M. Jiang, *Appl. Phys. Lett.* **72**, 1457 (1998).
- <sup>20</sup>N. A. Pertsev, A. G. Zembilgotov, and A. K. Tagantsev, *Phys. Rev. Lett.* **80**, 1988 (1998).
- <sup>21</sup>N. A. Pertsev, A. G. Zembilgotov, S. Hoffmann, R. Waser, and A. K. Tagantsev, *J. Appl. Phys.* **85**, 1698 (1999).
- <sup>22</sup>Landolt-Börnstein, *Numerical Data and Functional Relationships in Science and Technology*, edited by K.-H. Hellwege and A. M. Hellwege (Springler, Berlin, 1981), Vol. 16.
- <sup>23</sup>N. A. Pertsev, A. K. Tagantsev, and N. Setter, *Phys. Rev. B* **61**, R825 (2000).
- <sup>24</sup>T. Yamada, *J. Appl. Phys.* **43**, 328 (1972).
- <sup>25</sup>A. D. Hilton and B. W. Ricketts, *J. Phys. D* **29**, 1321 (1996).
- <sup>26</sup>M. E. Lines and A. M. Glass, *Principles and Applications of Ferroelectrics and Related Materials* (Clarendon, Oxford, 1977), p. 71.
- <sup>27</sup>W. D. Nix, *Metall. Trans. A* **20A**, 2217 (1989).
- <sup>28</sup>J. S. Speck and W. Pompe, *J. Appl. Phys.* **76**, 466 (1994).
- <sup>29</sup>S. P. Alpay and A. L. Roytburd, *J. Appl. Phys.* **83**, 4714 (1998).
- <sup>30</sup>S. P. Alpay, V. Nagarajan, A. Bendersky, M. D. Vaudin, S. Aggarwal, R. Ramesh, and A. L. Roytburd, *J. Appl. Phys.* **85**, 3271 (1999).
- <sup>31</sup>Landolt-Börnstein, *Numerical Data and Functional Relationships in Science and Technology*, edited by O. Madelung (Springler, Berlin, 1982), Vol. 17.
- <sup>32</sup>Y. Okada and Y. Tokumaru, *J. Appl. Phys.* **56**, 314 (1984).
- <sup>33</sup>M. McQuarrie, *J. Am. Chem. Soc.* **38**, 444 (1955).
- <sup>34</sup>C. Basceri, S. Streiffer, A. I. Kingon, and R. Waser, *J. Appl. Phys.* **82**, 2497 (1997).
- <sup>35</sup>N. A. Pertsev, V. G. Koukhar, R. Waser, and S. Hoffmann, *Appl. Phys. Lett.* **77**, 2596 (2000).
- <sup>36</sup>J. S. Speck, A. C. Daykin, A. Seifert, A. E. Romanov, and W. Pompe, *J. Appl. Phys.* **78**, 1696 (1995).
- <sup>37</sup>N. A. Pertsev and A. G. Zembilgotov, *J. Appl. Phys.* **78**, 6170 (1995).
- <sup>38</sup>N. A. Pertsev and A. G. Zembilgotov, *J. Appl. Phys.* **80**, 6401 (1996).
- <sup>39</sup>N. Sridhar, J. M. Rickman, and D. J. Srolovitz, *Acta Mater.* **44**, 4085 (1996).
- <sup>40</sup>N. Sridhar, J. M. Rickman, and D. J. Srolovitz, *Acta Mater.* **44**, 4097 (1996).
- <sup>41</sup>V. G. Koukhar, N. A. Pertsev, and R. Waser, *Phys. Rev. B* **64**, 214103 (2001).
- <sup>42</sup>B. S. Kwak, A. Erbil, J. D. Budai, M. F. Chrisholm, L. A. Boatner, and B. J. Wilkens, *Phys. Rev. B* **49**, 14865 (1994).
- <sup>43</sup>L. B. Freund, *MRS Bull.* **17**, 52 (1992).
- <sup>44</sup>L. B. Freund and W. D. Nix, *Appl. Phys. Lett.* **69**, 173 (1996).
- <sup>45</sup>D. R. Tilley and B. Žekš, *Solid State Commun.* **49**, 823 (1984).
- <sup>46</sup>D. R. Zhong, Y. G. Wang, P. L. Zhang, and B. D. Qu, *Phys. Rev. B* **50**, 698 (1994).
- <sup>47</sup>B. Jiang and L. A. Bursill, *Phys. Rev. B* **60**, 9978 (1999).
- <sup>48</sup>Y. G. Wang, W. L. Zhong, and P. L. Zhang, *Phys. Rev. B* **51**, 5311 (1995).
- <sup>49</sup>L.-H. Ong, J. Osman, and D. R. Tilley, *Phys. Rev. B* **63**, 144109 (2001).
- <sup>50</sup>J. Zhang, Z. Yin, M.-S. Zhang, and J. F. Scott, *Solid State Commun.* **118**, 241 (2001).
- <sup>51</sup>P. Ghosez and K. M. Rabe, *Appl. Phys. Lett.* **76**, 2767 (2000).
- <sup>52</sup>T. Tybell, C. H. Ahn, and J.-M. Triscone, *Appl. Phys. Lett.* **75**, 856 (1999).